Read the paper "Forty-seven Milky Way-Sized, Extremely Diffuse Galaxies in the Coma Cluster" by van Dokkum et al, and address the following questions. In general, I am looking for short (1-3 sentence) answers. I expect a passing grade will be 70-75 percent.

Gravitational constant  $G = 6.67^{-8} cm^3 gm^{-1} s^{-2}$ , Planck constant  $h = 6.63 \times 10^{-27} erg - s$ , speed of light  $c = 3 \times 10^{10} cm/s$ .

# 1. (15 points) Observations/measurements

- (a) Quantitatively, how does the limiting surface brightness of the experiment in the paper compare with that of the night sky, i.e. what is the flux ratio between the limiting surface brightness and the sky brightness?
  - Typical moonless night sky brightness is something like 22.5 mag/square arcsec in g. A surface brightness of 29.3 mag/square arcsec is 6.8 mag fainter, for a flux ratio of 0.002.
- (b) Why do you think the limiting surface brightness depends on the spatial scale?

  At such low surface brightness, the limitation is probably flat fielding, which becomes increasing uncertain at larger spatial scales.
- (c) Explain why a large difference between (fixed) aperture and SExtractor AUTO magnitudes rejects isolated stars and compact galaxies. What is the sense of this difference, i.e. is it m(AUTO) m(aperture) > 1.8 or m(aperture) m(AUTO) > 1.8?

  The AUTO magnitude is (presumably) based on surface brightness and extends farther out for an extended object. Point sources should have some fixed flux ratio (magnitude difference) between aperture and AUTO magnitude, while extended sources will have a larger ratio of AUTO flux to aperture flux. m(aperture) m(AUTO) > 1.8
- (d) The objects were detected with the Dragonfly Telephoto Array, but then required additional followup. What critical information does the CFHT followup provide?

  CFHT adds higher spatial resolution (0.8" instead of 6"), which is critical to determine that the Dragonfly objects are not a collection of different objects that average to a low surface brightness. Weeding out the spurious detections is required to see that the objects appear to be spatially associated with Coma.
- (e) What important additional information does the HST/ACS data provide?

  HST adds even higher spatial resolution, which supports the Coma association by showing that the objects are not resolved into individual stars, as they would be if they were closer.

## 2. (10 points) Ultra diffuse galaxies

(a) What known type of galaxies would these correspond to if they were not at the distance of Coma, i.e. if they were closer? What would be the closest Local Group analogs of these galaxies (if they were closer)?

These would be low surface brightness, low luminosity, small, red, spheroidal objects. Probably analogous to Local Group dwarf spheroidals.

- (b) What distance would these need to be at if they were members of the "normal" galaxy population? What absolute magnitude would they have at this distance?

  At Coma (100 Mpc) they have scale lengths of 1-4 kpc. To match low luminosity, low SB galaxies, perhaps they'd need to be 5-10 times smaller, i.e., at 10-20 Mpc. Luminosities would be 5 mag fainter than inferred at Coma.
- (c) What direction would these galaxies move in Figure 3 if they were closer? Constant surface brightness but smaller, i.e. they would move down.

## 3. (10 points) Galaxy properties

- (a) Explain why the colors do not uniquely indicate the age of the objects.

  There is an age-metallicity degeneracy in integrated color: objects can be bluer with older ages and lower metallicity or younger ages and higher metallicity.
- (b) Would different ages imply different stellar masses? Why or why not?

  Stellar mass-to-light ratios are larger for older populations, so you'd get more stellar mass than if you assumed a younger stellar population.

## 4. (20 points) Galaxy distributions

- (a) Describe and sketch the galaxy luminosity function, making sure to label the axes with quantities and numerical values. Indicate the location of the galaxies discussed in the paper.
  - Show typical shape of galaxy LF, with brightest galaxies around -23, and faintest around -8.
- (b) The galaxy luminosity function is usually parameterized by a Schechter function. Describe the parameters of this function, and give characteristic values for the general galaxy population. Write the functional form of the Schecter function.
  - Three parameters:  $\phi_*$ ,  $L_*$ , and  $\alpha$ . Functional form is exponential at high L, power law at low L.
- (c) What is known about the joint distributions of surface brightness and luminosity of the galaxy population? Make a sketch of the location of galaxies in a luminosity-surface brightness plane, remembering to label the axes with quantities and numerical values. Indicate the location of the galaxies discussed in the paper.
  - For elliptical sequence, higher luminosity is lower SB. For "disk" sequence, lower luminosity is lower SB.
- (d) The total luminosity of the entire galaxy population is important for accounting for how much of the baryonic content of the Universe is in stars. From the SDSS data in Figure 3, it looks like the surface brightness distribution at fixed radius is roughly flat between 20 and 22 g magnitudes per square arcsec. If the surface brightness distribution was flat out to 26 magnitudes per arcsec, how much additional luminosity (relative to a flat distribution only between 20 and 22) would exist in the total galaxy population?

Integrate

$$\int_{20}^{22} 10^{-0.4m} dm = \frac{1}{-0.4 \ln 10} \int_{20}^{22} \exp^{-0.4 \ln 10m} dm = \frac{1}{-0.4 \ln 10} (\exp^{-0.4 \ln 10(22)} - \exp^{-0.4 \ln 10(20)} = \frac{1}{-0.4 \ln 10} (\exp^{-0.4 \ln 10(20)} - \exp^{-0.4 \ln 10(20)} = \frac{1}{-0.4 \ln 10} (\exp^{-0.4 \ln 10(20)} - \exp^{-0.4 \ln 10(20)} = \frac{1}{-0.4 \ln 10} (\exp^{-0.4 \ln 10(20)} - \exp^{-0.4 \ln 10(20)} = \frac{1}{-0.4 \ln 10} (\exp^{-0.4 \ln 10(20)} - \exp^{-0.4 \ln 10(20)} = \frac{1}{-0.4 \ln 10} (\exp^{-0.4 \ln 10(20)} - \exp^{-0.4 \ln 10(20)} = \frac{1}{-0.4 \ln 10} (\exp^{-0.4 \ln 10(20)} - \exp^{-0.4 \ln 10(20)} = \frac{1}{-0.4 \ln 10} (\exp^{-0.4 \ln 10(20)} - \exp^{-0.4 \ln 10(20)} = \frac{1}{-0.4 \ln 10} (\exp^{-0.4 \ln 10(20)} - \exp^{-0.4 \ln 10(20)} = \frac{1}{-0.4 \ln 10} (\exp^{-0.4 \ln 10(20)} - \exp^{-0.4 \ln 10(20)} = \frac{1}{-0.4 \ln 10} (\exp^{-0.4 \ln 10(20)} - \exp^{-0.4 \ln 10(20)} = \frac{1}{-0.4 \ln 10} (\exp^{-0.4 \ln 10(20)} - \exp^{-0.4 \ln 10(20)} = \frac{1}{-0.4 \ln 10} (\exp^{-0.4 \ln 10(20)} - \exp^{-0.4 \ln 10(20)} = \frac{1}{-0.4 \ln 10} (\exp^{-0.4 \ln 10(20)} - \exp^{-0.4 \ln 10(20)} = \frac{1}{-0.4 \ln 10} (\exp^{-0.4 \ln 10(20)} - \exp^{-0.4 \ln 10(20)} = \frac{1}{-0.4 \ln 10} (\exp^{-0.4 \ln 10(20)} - \exp^{-0.4 \ln 10(20)} = \frac{1}{-0.4 \ln 10} (\exp^{-0.4 \ln 10(20)} - \exp^{-0.4 \ln 10(20)} = \frac{1}{-0.4 \ln 10} (\exp^{-0.4 \ln 10(20)} - \exp^{-0.4 \ln 10(20)} = \frac{1}{-0.4 \ln 10} (\exp^{-0.4 \ln 10(20)} - \exp^{-0.4 \ln 10(20)} = \frac{1}{-0.4 \ln 10} (\exp^{-0.4 \ln 10(20)} - \exp^{-0.4 \ln 10(20)} = \frac{1}{-0.4 \ln 10} (\exp^{-0.4 \ln 10(20)} - \exp^{-0.4 \ln 10(20)} = \frac{1}{-0.4 \ln 10} (\exp^{-0.4 \ln 10(20)} - \exp^{-0.4 \ln 10(20)} = \frac{1}{-0.4 \ln 10} (\exp^{-0.4 \ln 10(20)} - \exp^{-0.4 \ln 10(20)} = \frac{1}{-0.4 \ln 10} (\exp^{-0.4 \ln 10(20)} - \exp^{-0.4 \ln 10(20)} = \frac{1}{-0.4 \ln 10} (\exp^{-0.4 \ln 10(20)} - \exp^{-0.4 \ln 10(20)} = \frac{1}{-0.4 \ln 10} (\exp^{-0.4 \ln 10(20)} - \exp^{-0.4 \ln 10(20)} = \frac{1}{-0.4 \ln 10} (\exp^{-0.4 \ln 10(20)} - \exp^{-0.4 \ln 10(20)} = \frac{1}{-0.4 \ln 10} (\exp^{-0.4 \ln 10(20)} - \exp^{-0.4 \ln 10(20)} = \frac{1}{-0.4 \ln 10} (\exp^{-0.4 \ln 10(20)} - \exp^{-0.4 \ln 10(20)} = \frac{1}{-0.4 \ln 10} (\exp^{-0.4 \ln 10(20)} - \exp^{-0.4 \ln 10(20)} = \frac{1}{-0.4 \ln 10} (\exp^{-0.4 \ln 10(20)} - \exp^{-0.4 \ln 10(20)} = \frac{1}{-0.4 \ln 10} (\exp^{-0.4 \ln 10(20)} - \exp^{-0.4 \ln 10(20)} = \frac{1}{-0.4 \ln 10} (\exp^{-0.4 \ln 10(20)} - \exp^{-0.4 \ln 10(20)} = \frac{1}{-0.4 \ln 10} (\exp^{-0.4 \ln 10(20)} - \exp^{-0.4 \ln 10(20)} = \frac{1}{-0.4 \ln 10} (\exp^{-0.4 \ln 10($$

$$\int_{20}^{26} 10^{-0.4m} dm = \frac{1}{-0.4 \ln 10} \int_{20}^{22} \exp^{-0.4 \ln 10m} dm = \frac{1}{-0.4 \ln 10} (\exp^{-0.4 \ln 10(26)} - \exp^{-0.4 \ln 10(20)} = \frac{1}{-0.4 \ln 10} (\exp^{-0.4 \ln 10(26)} - \exp^{-0.4 \ln 10(20)} = \frac{1}{-0.4 \ln 10} (\exp^{-0.4 \ln 10(26)} - \exp^{-0.4 \ln 10(26)} = \frac{1}{-0.4 \ln 10} (\exp^{-0.4 \ln 10(26)} - \exp^{-0.4 \ln 10(26)} = \frac{1}{-0.4 \ln 10} (\exp^{-0.4 \ln 10(26)} - \exp^{-0.4 \ln 10(26)} = \frac{1}{-0.4 \ln 10} (\exp^{-0.4 \ln 10(26)} - \exp^{-0.4 \ln 10(26)} = \frac{1}{-0.4 \ln 10} (\exp^{-0.4 \ln 10(26)} - \exp^{-0.4 \ln 10(26)} = \frac{1}{-0.4 \ln 10} (\exp^{-0.4 \ln 10(26)} - \exp^{-0.4 \ln 10(26)} = \frac{1}{-0.4 \ln 10} (\exp^{-0.4 \ln 10(26)} - \exp^{-0.4 \ln 10(26)} = \frac{1}{-0.4 \ln 10} (\exp^{-0.4 \ln 10(26)} - \exp^{-0.4 \ln 10(26)} = \frac{1}{-0.4 \ln 10} (\exp^{-0.4 \ln 10(26)} - \exp^{-0.4 \ln 10(26)} = \frac{1}{-0.4 \ln 10} (\exp^{-0.4 \ln 10(26)} - \exp^{-0.4 \ln 10(26)} = \frac{1}{-0.4 \ln 10} (\exp^{-0.4 \ln 10(26)} - \exp^{-0.4 \ln 10(26)} = \frac{1}{-0.4 \ln 10} (\exp^{-0.4 \ln 10(26)} - \exp^{-0.4 \ln 10(26)} = \frac{1}{-0.4 \ln 10} (\exp^{-0.4 \ln 10(26)} - \exp^{-0.4 \ln 10(26)} = \frac{1}{-0.4 \ln 10} (\exp^{-0.4 \ln 10(26)} - \exp^{-0.4 \ln 10(26)} = \frac{1}{-0.4 \ln 10} (\exp^{-0.4 \ln 10(26)} - \exp^{-0.4 \ln 10(26)} = \frac{1}{-0.4 \ln 10} (\exp^{-0.4 \ln 10(26)} - \exp^{-0.4 \ln 10(26)} = \frac{1}{-0.4 \ln 10} (\exp^{-0.4 \ln 10(26)} - \exp^{-0.4 \ln 10(26)} = \frac{1}{-0.4 \ln 10} (\exp^{-0.4 \ln 10(26)} - \exp^{-0.4 \ln 10(26)} = \frac{1}{-0.4 \ln 10} (\exp^{-0.4 \ln 10(26)} - \exp^{-0.4 \ln 10(26)} = \frac{1}{-0.4 \ln 10} (\exp^{-0.4 \ln 10(26)} - \exp^{-0.4 \ln 10(26)} = \frac{1}{-0.4 \ln 10} (\exp^{-0.4 \ln 10(26)} - \exp^{-0.4 \ln 10(26)} = \frac{1}{-0.4 \ln 10} (\exp^{-0.4 \ln 10(26)} - \exp^{-0.4 \ln 10(26)} = \frac{1}{-0.4 \ln 10} (\exp^{-0.4 \ln 10(26)} - \exp^{-0.4 \ln 10(26)} = \frac{1}{-0.4 \ln 10} (\exp^{-0.4 \ln 10(26)} - \exp^{-0.4 \ln 10(26)} = \frac{1}{-0.4 \ln 10} (\exp^{-0.4 \ln 10(26)} - \exp^{-0.4 \ln 10(26)} = \frac{1}{-0.4 \ln 10} (\exp^{-0.4 \ln 10(26)} - \exp^{-0.4 \ln 10(26)} = \frac{1}{-0.4 \ln 10} (\exp^{-0.4 \ln 10(26)} - \exp^{-0.4 \ln 10(26)} = \frac{1}{-0.4 \ln 10} (\exp^{-0.4 \ln 10(26)} - \exp^{-0.4 \ln 10(26)} = \frac{1}{-0.4 \ln 10} (\exp^{-0.4 \ln 10(26)} - \exp^{-0.4 \ln 10(26)} = \frac{1}{-0.4 \ln 10} (\exp^{-0.4 \ln 10(26)} - \exp^{-0.4 \ln 10(26)} = \frac{1}{-0.4 \ln 10} (\exp^{-0.4 \ln 10(26)} - \exp^{-0.4 \ln 10(26)} = \frac{1}{-0.4 \ln 10} (\exp^{-0.4 \ln 10(26)} - \exp^{-0.4 \ln 10(26)} = \frac{1}{-0.4 \ln 10} (\exp^{-0.4 \ln 10($$

- 5. (10 points) Dark matter / galaxy evolution
  - (a) Derive the expression on the last page for the minimum total mass in the objects that are located near the core of the cluster (note that I don't reproduce it exactly!).

Tidal force at tidal radius equal to gravitational force:

$$\frac{GM_{gal}}{r_t^2} = \frac{2GMr_t}{R^3}$$

$$M_{gal} = 2M \frac{r_t^3}{R^3}$$

- (b) The final paragraph suggests that these could be disk galaxies that lost their gas by ram pressure stripping. What is ram pressure stripping and what quantities does its amplitude depend on? What observed property of these objects is not consistent with this hypothesis?
  - Ram pressure stripping is when pressure force on gas in an object from moving through a gaseous medium exceeds gravitational binding force. Proportional to density of medium and square of velocity of object through medium. But not clear how a disk with its gas removed gets turned into a spheroidal object!

## FORTY-SEVEN MILKY WAY-SIZED, EXTREMELY DIFFUSE GALAXIES IN THE COMA CLUSTER

PIETER G. VAN DOKKUM<sup>1</sup>, ROBERTO ABRAHAM<sup>2</sup>, ALLISON MERRITT<sup>1</sup>, JIELAI ZHANG<sup>2</sup>, Marla Geha<sup>1</sup>, and Charlie Conroy<sup>3</sup>

Department of Astronomy, Yale University, New Haven, CT 06511, USA <sup>2</sup> Department of Astronomy, University of Toronto, Toronto, ON M5S 3H4, Canada <sup>3</sup> Harvard-Smithsonian Center for Astrophysics, 60 Garden Street, Cambridge, MA 02138, USA Received 2014 October 27; accepted 2014 December 22; published 2015 January 7

### ABSTRACT

We report the discovery of 47 low surface brightness objects in deep images of a 3° × 3° field centered on the Coma cluster, obtained with the Dragonfly Telephoto Array. The objects have central surface brightness  $\mu(g,0)$  ranging from 24-26 mag arcsec<sup>-2</sup> and effective radii  $r_{\rm eff}=3''-10''$ , as measured from archival Canada-France-Hawaii Telescope images. From their spatial distribution we infer that most or all of the objects are galaxies in the Coma cluster. This relatively large distance is surprising as it implies that the galaxies are very large; with  $r_{\rm eff}=1.5-4.6\,{\rm kpc}$ their sizes are similar to those of  $L_*$  galaxies even though their median stellar mass is only  $\sim 6 \times 10^7 M_{\odot}$ . The galaxies are relatively red and round, with (g-i) = 0.8 and (b/a) = 0.74. One of the 47 galaxies is fortuitously covered by a deep Hubble Space Telescope Advanced Camera for Surveys (ACS) observation. The ACS imaging shows a large spheroidal object with a central surface brightness  $\mu_{475} = 25.8$  mag arcsec<sup>-2</sup>, a Sérsic index n = 0.6, and an effective radius of 7", corresponding to 3.4 kpc at the distance of Coma. The galaxy is not resolved into stars, consistent with expectations for a Coma cluster object. We speculate that these "ultra-diffuse galaxies" may have lost their gas supply at early times, possibly resulting in very high dark matter fractions.

Key words: galaxies: clusters: individual (Coma) - galaxies: evolution - galaxies: structure

#### 1. INTRODUCTION

While there have been tremendous advances in deep, highresolution imaging surveys over the past decades (e.g., Scoville et al. 2007; Heymans et al. 2012), the low surface brightness sky remains relatively unexplored. The Dragonfly Telephoto Array (Abraham & van Dokkum 2014) was developed with the specific aim of detecting low surface brightness emission. It is comprised of eight Canon 400 mm f/2.8 II telephoto lenses which all image the same part of the sky, forming what is effectively a 40 cm f/ 1.0 refractor. Four of the lenses are equipped with a Sloan Digital Sky Survey (SDSS) g filter and four with an SDSS r filter. The lenses are attached to cameras that provide an instantaneous field of view of  $2.6 \times 1.9$ , sampled with 2.8 pixels.

The main science program of Dragonfly is a deep imaging survey of a sample of nearby galaxies (see van Dokkum et al. 2014; Merritt et al. 2014). In the late spring of 2014 we interrupted this survey to observe the Coma cluster. The main goal of the Coma observation is to accurately measure the luminosity and color of the intra-cluster light (ICL). We are also looking for streams and tidal features, inspired by the beautiful deep imaging of the Virgo cluster of Mihos et al. (2005)

A visual inspection of the reduced images revealed a large number of faint, spatially resolved objects. The nature of these objects was not immediately obvious, as they are not listed in existing catalogs of faint galaxies in the Coma cluster (e.g., Ulmer et al. 1996; Adami et al. 2006). Furthermore, they seemed to be too large to be part of the cluster: typical dwarf galaxies have effective radii of a few hundred parsecs, which corresponds to much less than a Dragonfly pixel at the distance of Coma  $(D_A = 98 \,\mathrm{Mpc}; D_L = 103 \,\mathrm{Mpc}).$ 

dwarf galaxies in the foreground of the cluster, we decided

Expecting that the objects would turn out to be isolated

to perform a (mostly) objective selection with the aid of SDSS and archival Canada-France-Hawaii Telescope (CFHT) data, as described in the next section. Surprisingly, as we show below, the objects turn out to be associated with the Coma cluster after all, and represent a class of very large, very diffuse galaxies. Only a handful of similar objects were known from previous studies (Impey et al. 1988; Bothun et al. 1991; Dalcanton et al. 1997).

# 2. IDENTIFICATION

#### 2.1. Candidates in the Dragonfly Data

The Coma cluster was observed for 26 hr, obtained over 25 nights in the period March-May 2014. The images were reduced using standard techniques, as described in van Dokkum et al. (2014) and Merritt et al. (2014), and projected onto a common astronometric frame with 2".0 pixels. Owing to large dithers between individual exposures, the final g and r images span 3.33  $\times$  3.33, centered on  $\alpha = 12^{h}59^{m}48.8$ ,  $\delta = 27^{\circ}58'51''$ . The FWHM image quality varies somewhat over the field, but is typically  $\approx 6''$ . The limiting depths in the images depend on the spatial scale; on the 10" scales relevant for this Letter the  $1\sigma$  limits are  $\mu(g) \sim 29.3$  mag arcsec<sup>-2</sup> and  $\mu(r) \sim 28.6 \,\mathrm{mag \, arcsec^{-2}}$ .

We used SExtractor (Bertin & Arnouts 1996) to create an initial catalog of 102,209 objects in the Dragonfly field. The g and r images were summed to increase the signal-to-noise ratio (S/N) in the detection image. For each object two magnitudes were measured: one based on the flux in SExtractor's "AUTO" aperture, and one in an aperture with a fixed diameter of 6". Objects were flagged as possible low surface brightness galaxies (LSBs) if their aperture magnitude is in the range 20 < AB < 23 and the difference between the AUTO and aperture magnitude exceeds 1.8. The latter criterion rejects isolated stars and compact galaxies, leaving 6624 objects that are faint and extended at the Dragonfly resolution.

 $<sup>^4</sup>$  Assuming  $cz=7090~\rm km~s^{-1}$  (Geller et al. 1999) and a Hubble constant of  $70~\rm km~s^{-1}~Mpc^{-1}$ 

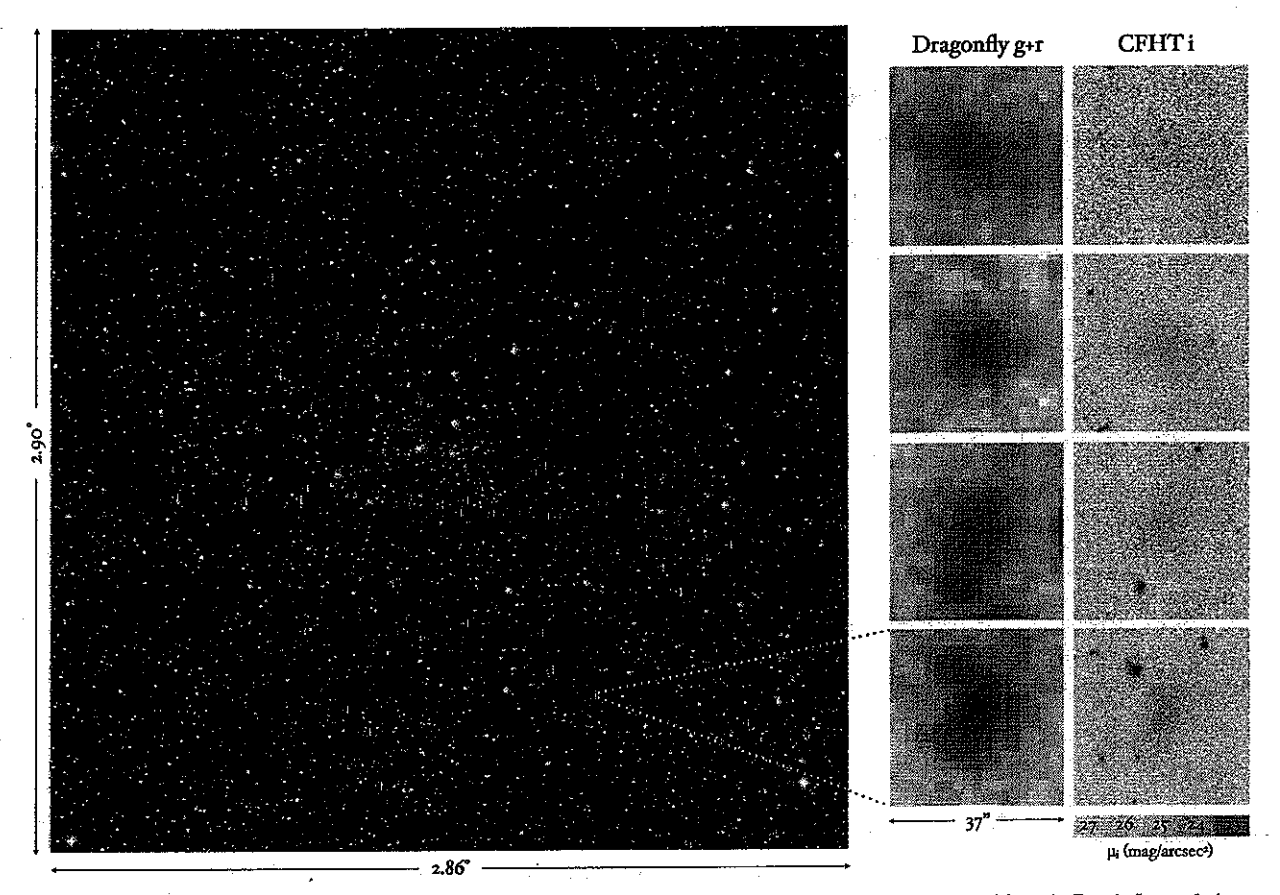


Figure 1. Main panel: spatial distribution of the newly discovered galaxies, projected on a color image of the Coma cluster created from the Dragonfly g and r images. Only the  $2.86 \times 2.90$  area that is covered by CFHT imaging is shown. Panels at right: typical examples of the galaxies, spanning a range in brightness.

## 2.2. Rejection Using SDSS and CFHT

The vast majority of the 6624 objects are not LSBs but groups of neighboring galaxies, or stars and galaxies, that are single objects at the Dragonfly resolution. We removed most of these by requiring that there is no object in the SDSS catalog within 4" of the Dragonfly position, leaving 344 candidates.

The SDSS imaging does not have sufficient depth and spatial resolution to identify faint groups of galaxies. We obtained CFHT imaging of the Coma field from the Canadian Astronomy Data Centre. A  $3^{\circ} \times 3^{\circ}$  field was imaged with a 9-pointing mosaic in the g and i bands (Head et al. 2014). Exposure times were short, at 300 s per pointing per filter, but the image quality (FWHM  $\approx 0''.8$ ) and sampling (0''.186 pixel<sup>-1</sup>) are far superior to the Dragonfly and SDSS imaging. We created  $37'' \times 37''$  cutouts of all 344 candidates and used SExtractor to identify cases where multiple moderately bright (i < 22.5) objects are detected within 7'' of the Dragonfly position. This step left 186 objects which were inspected by eye. Of these, 139 were rejected, with most turning out to be clumps of multiple objects fainter than the i = 22.5 limit.

## 2.3. A Population of Large, Diffuse Galaxies

We are left with 47 objects, listed in Table 1, that are clearly detected in the Dragonfly imaging, are spatially extended, are not detected in the SDSS, and do not resolve into multiple objects in the higher resolution CFHT data. Four typical examples spanning a range of apparent brightness are shown in Figure 1.

The galaxies are clearly detected but barely resolved in the Dragonfly data, and very faint, fuzzy blobs in the CFHT data.

We had expected that the objects would be randomly distributed in the 3° × 3° field that has both Dragonfly and CFHT coverage, as their apparent sizes seemed too large for a distance of 100 Mpc. However, as shown in Figure 1 they are strongly clustered toward the center of the image. A Monte Carlo implementation of the Clark-Evans test gives a probability of 0.04% that the distribution is spatially random. Moreover, the apparent east-west elongation of the distribution is similar to that of confirmed Coma cluster members (e.g., Doi et al. 1995). We conclude that most or all of the LSBs are, in fact, at the distance of the Coma cluster and are resolved in the Dragonfly data because they are intrinsically very large. As we show in Section 4 this conclusion is supported by *Hubble Space Telescope (HST)* Advanced Camera for Surveys (ACS) imaging of one of the galaxies.

#### 3. PROPERTIES

#### 3.1. Structure

We used GALFIT (Peng et al. 2002) to measure structural parameters of the galaxies from the CFHT images. The fits were performed on the summed g+i images, with neighboring objects masked. To increase the stability of the fits, the Sérsic index and sky background were not allowed to vary. All galaxies were fit three times, with the Sérsic index held fixed at n=0.5, n=1, and n=1.5. The average  $\chi^2$  is lowest for n=1

Table 1
Positions and Properties

Positions and Properties						
Id	R.A. (J2000)	Decl. (J2000)	$\mu(g,0)$ (mag arcsec <sup>-2</sup> )	r <sub>eff</sub> (kpc)	M <sub>g</sub> (mag)	b/a
DF1	12h59m14s1	29°07′16″	25.1 <sup>+0.5</sup> <sub>-0.5</sub>	3.1+0.9	$-14.6^{+0.3}_{-0.2}$	$0.82 \pm 0.03$
DF2	12h59m0955	29°00′25″	24.4 <sup>+0.6</sup>	$2.1^{+0.6}_{-0.4}$	$-14.3^{+0.2}_{-0.2}$	$0.71 \pm 0.03$
DF3	13h02m165	28°57′17″	$24.5^{+0.5}_{-0.5}$	$2.9^{+0.8}_{-0.7}$	$-14.2^{+0.3}_{-0.2}$	$0.40 \pm 0.04$
DF4	13h02m33s4	28°34′51″	25.7 <sup>+0.6</sup>	3.9 <sup>+1.0</sup>	$-14.3^{+0.2}_{-0.2}$	$0.71 \pm 0.03$
DF5	12h55m1055	28°33′32″	24.9 <sup>+0.6</sup>	$1.8^{+0.4}_{-0.4}$	$-13.5^{+0.2}_{-0.2}$	$0.71 \pm 0.03$
DF6	12h56m29s7	28°26′40″	25.5 <sup>+0.5</sup> <sub>-0.5</sub>	$4.4^{+1.6}_{-1.1}$	$-14.3^{+0.4}_{-0.3}$	$0.47\pm0.03$
DF7	12h57m01s7	28°23′25″	24.4 <sup>+0.5</sup>	$4.3^{+1.4}_{-0.8}$	$-16.0^{+0.2}_{-0.2}$	$0.76 \pm 0.03$
DF8	13h01m3054	28°22′28″	25.4 <sup>+0.5</sup>	$4.4^{+1.5}_{-0.9}$	$-14.9^{+0.3}_{-0.3}$	$0.73 \pm 0.05$
DF9	12h56m22s8	28°19′53″	25.6 <sup>+0.7</sup> <sub>0.7</sub>	$2.8^{+0.5}_{-0.4}$	14.0 <sup>+0.1</sup>	$0.92 \pm 0.03$
DF10	12 <sup>h</sup> 59 <sup>m</sup> 1 <del>6</del> ?3	28°17′51″	24.4 <sup>+0.6</sup>	$2.4^{+0.6}_{-0.4}$	$-14.7^{+0.2}_{-0.2}$	$0.83 \pm 0.03$
DF11	13h02m25.5	28°13′58″	$24.2^{+0.6}_{-0.6}$	$2.1^{+0.4}_{-0.3}$	$-14.8^{+0.2}_{-0.1}$	$0.98 \pm 0.03$
DF12	13h00m09s1	28°08′27″	25.2 <sup>+0.6</sup>	$2.6^{+0.6}_{-0.9}$	$-14.1^{+0.5}_{-0.2}$	$0.88 \pm 0.03$
DF13	13 <sup>h</sup> 01 <sup>m</sup> 56.2	28°07′23″	$25.3^{+0.6}_{-0.6}$	$2.2^{+0.6}_{-0.5}$	$-13.7^{+0.3}_{-0.2}$	$0.83 \pm 0.03$
DF14	12h58m07s8	27°54′46″	25.3 <sup>+0.7</sup> <sub>-0.7</sub>	$3.8^{+0.8}_{-0.1}$	$-14.4^{+0.1}_{-0.1}$	$0.51 \pm 0.07$
DF15	12 <sup>h</sup> 58 <sup>m</sup> 16:3	27°53′29″	$25.5^{+0.1}_{-0.1}$	$4.0^{+5.5}_{-0.1}$	$-14.9^{+0.1}_{-0.4}$	$0.99 \pm 0.29$
DF16	12h56m52s4	27°52′29″	24.8 <sup>+0.8</sup> <sub>-0.8</sub>	$1.5^{+0.1}_{-0.2}$	$-13.2^{+0.2}_{-0.1}$	$0.82 \pm 0.10$
DF17	13h01m5893	27°50′11″	$25.1^{+0.5}_{-0.5}$	$4.4^{+1.5}_{-0.9}$	$-15.2^{+0.3}_{-0.2}$	$0.71 \pm 0.03$
DF18	12h59m09s3	27°49′48″	25.5 <sup>+0.6</sup>	$2.8^{+0.6}_{-0.5}$	$-13.4^{+0.2}_{-0.1}$	$0.47 \pm 0.03$
DF19	13 <sup>h</sup> 04 <sup>m</sup> 05 <sup>s</sup> .1	27°48′05″	25.9 <sup>+0.5</sup>	4.4 <sup>+1.6</sup>	$-14.5^{+0.3}_{-0.3}$	$0.78 \pm 0.03$
DF20	13 <sup>h</sup> 00 <sup>m</sup> 18 <sup>s</sup> 9	27°48′06″	25.5+0.8	$2.3_{-0.1}^{+0.3}$	$-13.0^{+0.1}_{-0.1}$	$0.53 \pm 0.11$
DF21	13h02m04s1	27°47′55″	$23.5^{+0.7}_{-0.7}$	$1.5^{+0.3}_{-0.2}$	$-14.6^{+0.2}_{-0.1}$	$0.82 \pm 0.03$
DF22	13 <sup>h</sup> 02 <sup>m</sup> 57 <sup>s</sup> 8	27°47′25″	$25.1^{+0.6}_{-0.6}$	$2.1^{+0.4}_{-0.3}$	$-13.8^{+0.2}_{-0.1}$	$0.84 \pm 0.03$
DF23	12h59m23s8	27°47′27″	$24.8^{+0.6}_{-0.6}$	2.3 <sup>+0.5</sup>	$-14.3^{+0.2}_{-0.2}$	$0.89 \pm 0.03$
DF24	12h56m28s9	27°46′19″	$25.2^{+0.7}_{-0.7}$	$1.8^{+0.4}_{-0.4}$	$-12.5^{+0.2}_{-0.2}$	$\boldsymbol{0.38 \pm 0.03}$
DF25	12 <sup>h</sup> 59 <sup>m</sup> 48 <sup>s</sup> .7	27°46′39″	25.2 <sup>+0.5</sup>	$4.4^{+1.4}_{-0.7}$	$-14.5^{+0.2}_{-0.2}$	$0.43 \pm 0.03$
DF26	13h00m20s6	27°47′13″	$24.1^{+0.6}_{-0.6}$	$3.3^{+0.8}_{-0.4}$	$-15.4^{+0.2}_{-0.2}$	$0.63 \pm 0.03$
DF27	12h58m57f3	27°44′39″	$\gtrsim 26.5$	•••	•••	•••
DF28	12h59m30s4	27°44′50″	24.4 <sup>+0.6</sup> <sub>-0.6</sub>	$2.7^{+0.6}_{-0.4}$	$-14.9^{+0.2}_{-0.2}$	$0.79 \pm 0.03$
DF29	12h58m05s0	27°43′59″	$25.3^{+0.2}_{-0.2}$	$3.1^{+1.6}_{-0.1}$	14.6 <sup>+0.1</sup>	$0.99 \pm 0.13$
DF30	12h53m15i1	27°41′15″	$24.4^{+0.5}_{-0.5}$	$3.2^{+0.9}_{-0.6}$	$-15.2^{+0.2}_{-0.2}$	$0.70 \pm 0.03$
DF31	12h 55m 06.2	27°37′27″	25.0+0.5	$2.5^{+0.7}_{-0.6}$	$-14.1^{+0.3}_{-0.2}$	$0.75 \pm 0.03$
DF32	12h56m28s4	27°37′06″	$24.8^{+0.6}_{-0.6}$	$2.8^{+0.6}_{-0.3}$	$-14.2^{+0.1}_{-0.1}$	$0.52 \pm 0.03$
DF33	12h55m30s1	27°34′50″	$25.1^{+0.7}_{-0.7}$	$1.9^{+0.2}_{-0.1}$	$-13.4^{+0.1}_{-0.1}$	$0.69 \pm 0.03$
DF34	12 <sup>h</sup> 56 <sup>m</sup> 12 <sup>s</sup> 9	27°32′52″	$26.0^{+0.6}_{-0.6}$	$3.4^{+0.5}_{-0.4}$	$-13.6^{+0.1}_{-0.1}$	$0.66 \pm 0.03$
DF35	13 <sup>h</sup> 00 <sup>m</sup> 35 <sup>s</sup> .7	27°29′51″	$25.6^{+0.4}_{-0.4}$	$2.7^{+1.0}_{-0.3}$	$-13.9^{+0.2}_{-0.2}$	$0.89 \pm 0.09$
DF36	12h55m55s.4	27°27′36″	25.0 <sup>+0.6</sup>	$2.6^{+1.0}_{-0.4}$	$-14.3^{+0.3}_{-0.4}$	$0.80\pm0.14$
DF37	12 <sup>h</sup> 59 <sup>m</sup> 23 <sup>s</sup> 6	27°21′22″	$24.5^{+0.7}_{-0.7}$	$1.5^{+0.3}_{-0.2}$	$-13.7^{+0.2}_{-0.2}$	$0.83 \pm 0.03$
DF38	13h02m00s1	27°19′51″	$24.2^{+0.6}_{-0.6}$	$1.8^{+0.4}_{-0.3}$	$-14.3^{+0.2}_{-0.1}$	$0.84 \pm 0.03$
DF39	12h58m10s4	27°19′11″	25.5 <sup>+0.5</sup>	$4.0^{+1.3}_{-0.7}$	$-14.7^{+0.2}_{-0.2}$	$0.77 \pm 0.05$
DF40	12 <sup>h</sup> 58 <sup>m</sup> 01 <sup>s</sup> 1	27°11′26″	$24.6^{+0.6}_{-0.6}$	$2.9_{-0.5}^{+0.7}$	$-14.6^{+0.2}_{-0.2}$	$0.56 \pm 0.03$
DF41	12 <sup>h</sup> 57 <sup>m</sup> 19 <sup>s</sup> 0	27°05′56″	$24.9^{+0.5}_{-0.5}$	$3.4^{+0.9}_{-0.5}$	$-14.7^{+0.1}_{-0.1}$	$0.64 \pm 0.03$
DF42	13h01m1951	27°03′15″	25.0 <sup>+0.6</sup>	2.9 <sup>+0.6</sup>	$-14.1^{+0.1}_{-0.1}$	$0.52 \pm 0.03$
DF43	12h54m51s4	26°59′46″	$24.2^{+0.8}_{-0.8}$	$1.5^{+0.2}_{-0.2}$	$-13.8^{+0.2}_{-0.2}$	$0.82 \pm 0.10$
DF44	13 <sup>h</sup> 00 <sup>m</sup> 58 <sup>s</sup> 0	26°58′35″	24.5 <sup>+0.5</sup> <sub>-0.5</sub>	$4.6^{+1.5}_{-0.8}$	$-15.7^{+0.2}_{-0.2}$	$0.65 \pm 0.03$
DF45	12h53m539.7	26°56′48″	24.4 <sup>+0.5</sup> <sub>-0.5</sub>	$1.9^{+0.6}_{-0.4}$	$-14.2^{+0.2}_{-0.2}$	$0.80 \pm 0.03$
DF46	13 <sup>h</sup> 00 <sup>m</sup> 47 <sup>s</sup> 3	26°46′59″	$25.4^{+0.6}_{-0.6}$	$3.4^{+1.0}_{-0.6}$	$-14.4^{+0.2}_{-0.2}$	$0.74 \pm 0.04$
DF47	12h55m48s1	26°33′53″	$25.5^{+0.5}_{-0.5}$	$4.2^{+1.4}_{-0.7}$	$-14.6^{+0.1}_{-0.2}$	$0.66 \pm 0.04$

(exponential), but for individual galaxies the three fits are generally equally good. We therefore use the n=1 results for all objects and determine the uncertainties in the structural parameters of individual galaxies from the full range of fits. Three examples of fits are shown in Figure 2. Forty-six galaxies

were successfully fit; the S/N of one object (DF27) is too low for a stable fit.

The distribution of the galaxies in the surface brightness—size plane is shown in Figure 3, under the assumption that they are all at the distance of the Coma cluster. The central

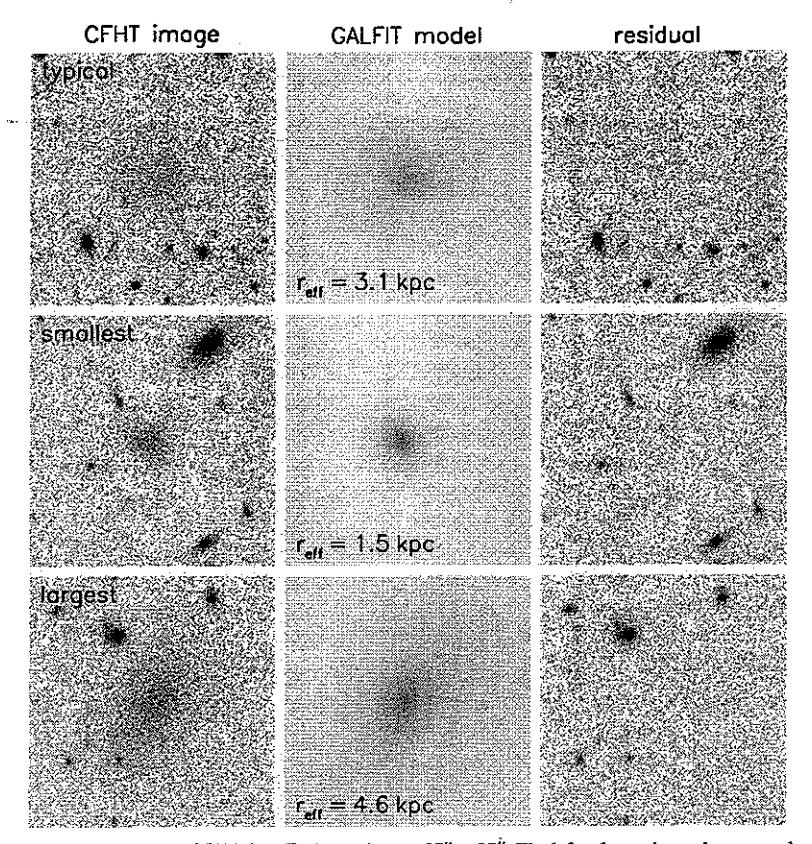


Figure 2. Examples of structural parameter fits to the CFHT data. Each panel spans  $37'' \times 37^{j'}$ . The left column shows the summed g+i images, the middle column shows the best-fitting GALFIT models (with n=1), and the right column shows the residuals from the fits. The size and surface brightness of the galaxy in the top (DF1) row are close to the median of the sample. The middle row shows the smallest galaxy in the sample (DF43), and the bottom row shows the largest (DF44).

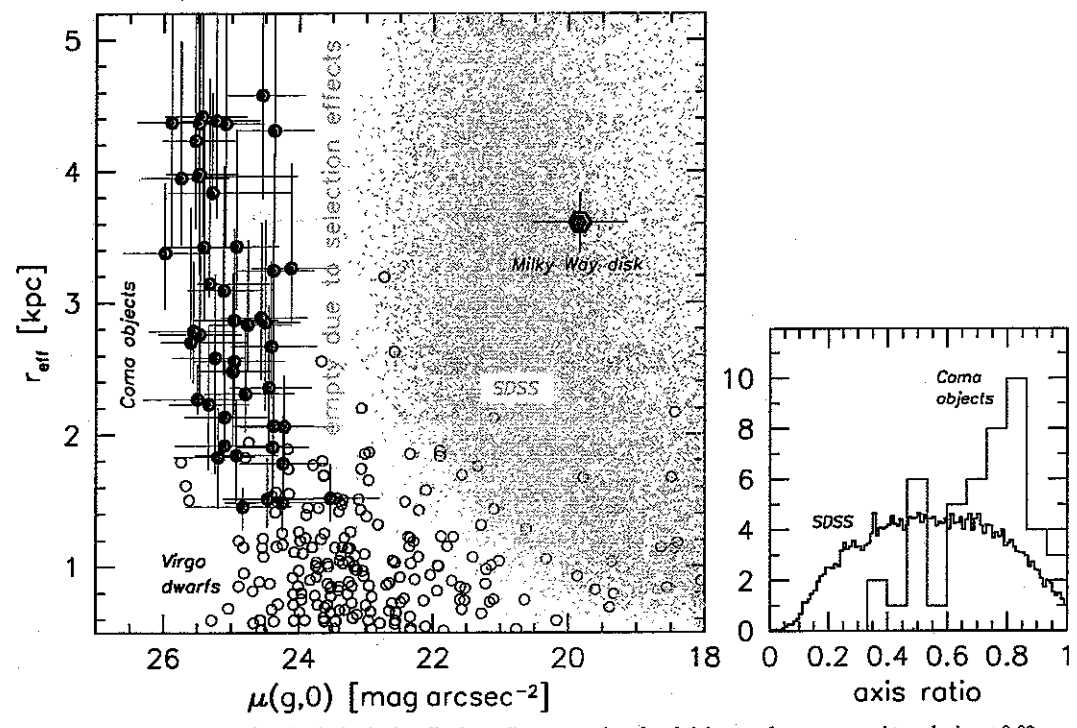


Figure 3. Main panel: location of the newly found galaxies in the effective radius—central surface brightness plane, compared to galaxies at 0.02 < z < 0.03 in the SDSS (Simard et al. 2011), early-type galaxies in the Virgo cluster (Gavazzi et al. 2005), and the disk of the Milky Way (Bovy & Rix 2013). Right panel: axis ratio distribution compared to that of similar-sized SDSS galaxies.

surface brightnesses, calculated from the circularized effective radii and the total fit magnitudes, range from  $\mu(g,0) =$ 24-26 mag arcsec<sup>-2</sup>. The effective radii, measured along the major axis, range from 1.5 kpc to 4.5 kpc. At fixed surface brightness the newly found galaxies are much larger than typical dwarf elliptical galaxies in the Virgo cluster (open circles; Gavazzi et al. 2005). The median central surface brightness  $\langle \mu(g,0) \rangle = 25.0 \,\mathrm{mag \, arcsec^{-2}} \ (\approx 25.4 \,\mathrm{mag \, arcsec^{-2}} \ \mathrm{in \, the} \ B$ band) and the median effective radius  $\langle r_{\rm eff} \rangle = 2.8 \, \rm kpc$ . An interesting point of comparison is the disk of the Milky Way. Bovy & Rix (2013) derive a mass-weighted exponential scale length of  $2.15 \pm 0.14$  kpc, corresponding to  $r_{\text{eff}} = 3.6$  kpc. Twelve of the newly found objects are larger than this, although for individual objects the difference is typically not significant. We note that the gap between SDSS and the Dragonfly data in Figure 3 is due to the selection limits of the surveys. The newly found galaxies are simply the low surface brightness, large size extension of the general galaxy population, and samples such as that of Thompson & Gregory (1993) would fill in the gap.

The axis ratio distribution is shown in the right panel of Figure 3. The galaxies are remarkably round, with a median axis ratio of 0.74. We note that there is no obvious selection effect against inclined disks, as the galaxies are barely resolved in the Dragonfly data. Randomly oriented thin disks would have a uniform b/a distribution, and this can be ruled out.

## 3.2. Stellar Content

The median absolute g band magnitude  $\langle M_g \rangle = -14.3$ . The average color of the galaxies  $\langle g-i \rangle = 0.8 \pm 0.1$ , as measured from stacks of the CFHT g and i images. Their colors are similar to those of the reddest Milky Way globular clusters (Vanderbeke et al. 2014), and consistent with an extrapolation of the red sequence of early-type galaxies in Coma (Gavazzi et al. 2010). The observed color is consistent with a passively evolving stellar population with a low metallicity and/or a relatively young age. For example, the Conroy et al. (2009) models predict g-i=0.8 for an age of 7 Gyr and [Fe/H] = -1.4, and for an age of 4 Gyr and [Fe/H] = -0.8 (see also Michielsen et al. 2008).

From the absolute magnitudes and colors we can estimate the stellar masses of the galaxies. The absolute magnitudes range from  $-16.0 \le M_g \le -12.5$ ; using Equation (8) in Taylor et al. (2011) with g-i=0.8, we find that the galaxies have stellar masses in the range  $1\times 10^7\,M_\odot - 3\times 10^8\,M_\odot$ . The median stellar mass  $\langle M_{\rm star}\rangle \sim 6\times 10^7\,M_\odot$ , and the median stellar density within the effective radius is  $\sim 5\times 10^5\,M_\odot$  kpc<sup>-3</sup>.

## 4. DEEP HST/ACS IMAGING

We searched the *HST* Archive for serendipitous observations of the newly found galaxies. Three of the 47 galaxies have been observed by *HST*. Two of the observations are short (200–300 s) WFPC2 exposures, which show only hints of the objects. The third comprises 8 orbit, multi-band ACS imaging of DF17, whose properties are close to the median of the sample. The ACS data include  $g_{475}$ ,  $V_{606}$ , and  $I_{814}$  parallels to a Cepheid program with the WFC3/UVIS camera (GO-12476, PI: Cook; Macri et al. 2013). The data were obtained from the archive and reduced using standard techniques (van Dokkum 2001).

A color image, created from the  $V_{606}$  and  $I_{814}$  images, is shown in Figure 4. DF17 is large and spheroidal and does not have obvious spiral arms, star forming regions, or tidal features. We fit the ACS data with a Sérsic profile, leaving all parameters free. The best fitting parameters are  $r_{\rm eff} = 7''.0$ , n = 0.6,  $\mu_{475} = 25.8$ ,

and b/a = 0.71. The effective radius, surface brightness, and axis ratio are in excellent agreement with the n = 0.5 fit to the CFHT image.

The fact that the galaxy is not resolved into stars implies a lower limit to its distance. We created model images of DF17, following the methodology described in van Dokkum & Conroy (2014). Stars were drawn randomly from a Poisson distribution, weighted by their expected frequency in a 10 Gyr old stellar population with a metallicity [Fe/H] = -1.6. This stellar population reproduces the observed  $V_{606} - I_{814}$  color ( $V_{606} - I_{814} = 0.40$ ). The models are constrained to reproduce the observed two-dimensional light distribution of DF17 and its observed total magnitude of  $I_{814} = 19.3$ , with the distance as the only free parameter. The model images were convolved with the ACS point-spread function and placed in the ACS image, after subtracting the best-fitting GALFIT model of the galaxy.

The results are shown in the bottom panels of Figure 4. Out to well beyond the Virgo cluster (16 Mpc) the ACS camera easily resolves individual stars in LSBs, as also shown by Caldwell (2006). Only at distances  $\gtrsim 50\,\mathrm{Mpc}$  do the models take on the same smooth appearance as the data, and we conclude that the ACS observations support the interpretation that the galaxies are associated with the Coma cluster. The effective radius of DF17 is then 3.4 kpc, almost identical to that of the disk of the Milky Way.

### 5. DISCUSSION

We have identified a significant population of low surface brightness, red, nearly round objects in a wide field centered on the Coma cluster. Based on their spatial distribution and the analysis of one example observed with ACS, we infer that most or all of the objects are associated with Coma. Their inferred sizes are similar to those of  $L_*$  galaxies and the disk of the Milky Way, even though their stellar masses are a factor of  $\sim 10^3$  lower.

The galaxies do not resemble "classical" LSBs such as those described by, e.g., van der Hulst et al. (1993), Bothun et al. (1997), and van den Hoek et al. (2000). Typical LSBs have blue, gas-rich disks, and are thought to be normal spiral galaxies with a low stellar content and low star formation rate for their rotation velocity (see, e.g., Schombert et al. 2013, and references therein). They are also significantly brighter than the objects found in this Letter: the lowest surface brightness object in the compilation of Bothun et al. (1997) has  $\mu(0, B) \approx 24.0 \,\mathrm{mag\,arcsec^{-2}}$ , corresponding to  $\mu(0, g) \approx 23.6 \,\mathrm{mag\,arcsec^{-2}}$ . Many have bulges; for example, Malin I has a central surface brightness  $\lesssim 16 \,\mathrm{mag\,arcsec^{-2}}$  if its bulge is taken into account (Lelli et al. 2010).

Visually and structurally, the newly found galaxies are more similar to dwarf spheroidal galaxies such as those found in the Local Group, around M101, and in the Virgo and Coma clusters than to classical LSBs: they have similar Sérsic indices, axis ratios, and surface brightness (e.g., Thompson & Gregory 1993; Geha et al. 2003; Gavazzi et al. 2005; McConnachie 2012; Merritt et al. 2014; Toloba et al. 2014). However, the term "dwarf" is not appropriate for these large objects. Dwarf spheroidals have typical sizes of a few hundred parsecs (e.g., McConnachie 2012; Lieder et al. 2012), and in the Local Group and other nearby groups only a few have an effective radius exceeding 1 kpc (e.g., Kim et al. 2011; McConnachie 2012; Chiboucas et al. 2013; Merritt et al. 2014). The largest known low luminosity Local Group galaxy is And XIX, with a size of 1.6 kpc (McConnachie et al. 2008). The Coma objects are much

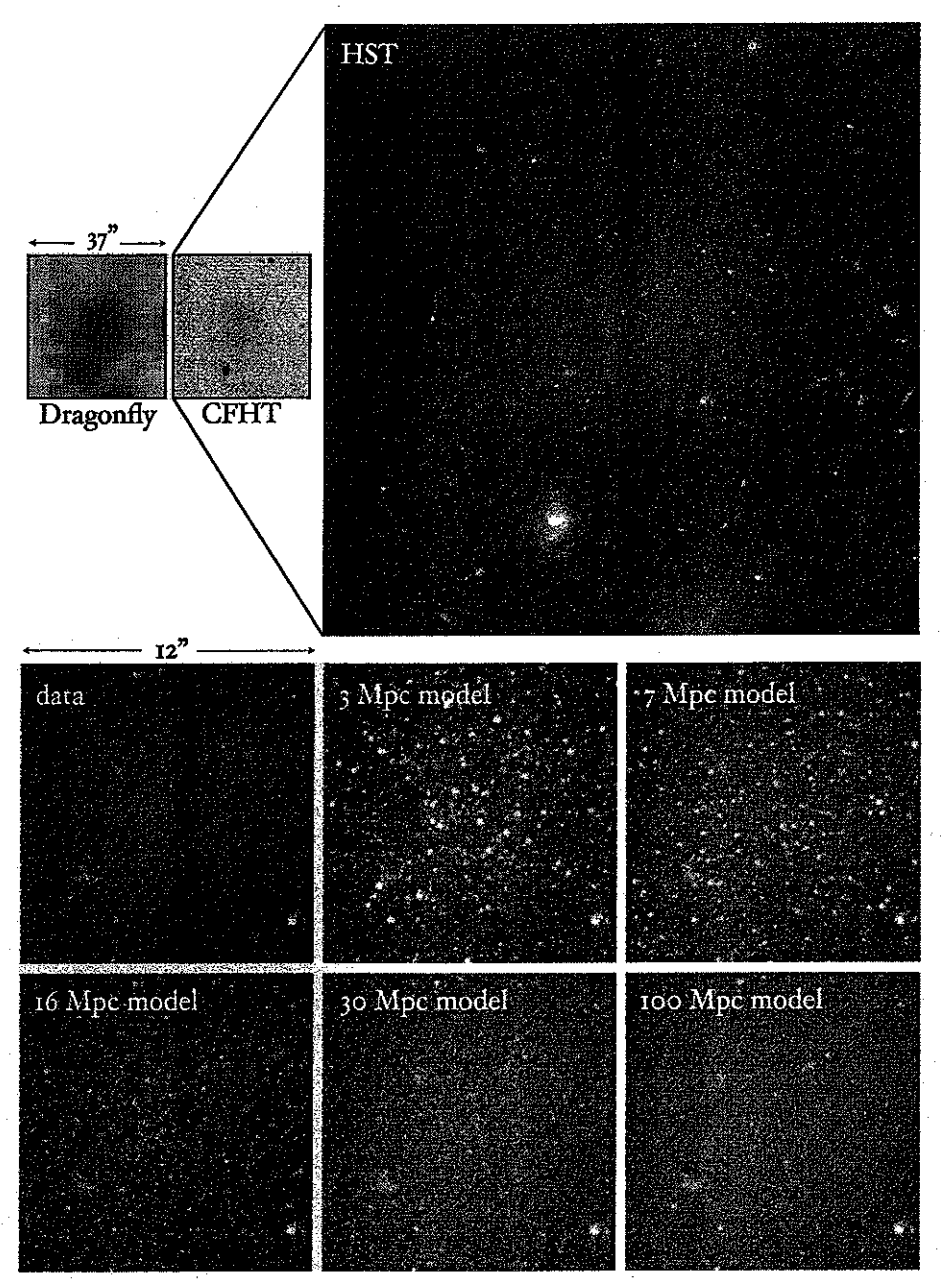


Figure 4. One of the galaxies, DF17, has been observed with ACS on HST. The main panel shows a color image created from the  $V_{606}$  and  $I_{814}$  ACS images. The galaxy is smooth, red, spheroidal, and is not resolved into stars. The bottom panels show the expected appearance of the galaxy for different distances (see text). The ACS data are consistent with the Coma distance of  $\approx 100$  Mpc.

larger, with sizes typical of  $\sim L_*$  spiral and elliptical galaxies (e.g., Shen et al. 2003).

The closest analogs to the Coma objects are several very large low surface brightness objects in the Virgo and Fornax clusters, first identified by Impey et al. (1988). There are four galaxies in the Impey et al. sample with central surface brightness  $\geq$ 25 mag arcsec<sup>-2</sup> and  $r_{\rm eff} > 2.5$  kpc; the largest of these, V1L5 and V4L7, have  $r_{\rm eff} = 3.7$  kpc. As the Impey et al. survey area is four times smaller than ours the number of such galaxies in Virgo and Coma could be similar. Although the distances to these particular objects are not confirmed, Caldwell (2006) used HST/ACS imaging to show that at least one galaxy with a central

surface brightness of  $\mu(g,0) \approx 27.2$  and an effective radius of 1.5 kpc is part of the Virgo cluster. We propose the term "ultradiffuse galaxies," or UDGs, for galaxies with  $r_e \gtrsim 1.5$  kpc and  $\mu(g,0) \gtrsim 24$  mag arcsec<sup>-2</sup>. We stress that this term does not imply that these objects are distinct from the general galaxy population; these are simply the largest and most diffuse objects in a continuous distribution.

As shown in Figure 5 no UDGs are found in the central regions of the cluster, consistent with earlier results for slightly brighter diffuse spheroidals in Coma (Thompson & Gregory 1993). This could mean that they are only able to survive at large radii (see, e.g., Bothun et al. 1991; Gregg & West 1998; Martel et al. 2012).



Figure 5. Central 0°89 × 0°70 (1.6 Mpc × 1.2 Mpc) of the Dragonfly image shown in Figure 1. The newly found galaxies appear to avoid the region where ICL is detected.

We can estimate what the mass of the galaxies needs to be to survive a passage within  $\sim 300 \,\mathrm{kpc}$  of the core of the cluster, which is where the closest-in UDGs are located. The criterion for survival is that the total mass  $m_{\mathrm{tot}}$  within the tidal radius  $r_{\mathrm{tide}} = 2r_e = 6 \,\mathrm{kpc}$  is at least  $m_{\mathrm{tot}} > 3M(r_{\mathrm{tide}}/R)^3$ , with M the mass of the cluster within radius R. Using the mass profile of A2667 (Newman et al. 2013) as a proxy for that of Coma, we find  $m_{\mathrm{tot}} \gtrsim 3 \times 10^9 \,M_{\odot}$ , or a dark matter fraction within the tidal radius of  $\gtrsim 98\%$ . We note that there may be UDGs closer to the cluster core, as crowding and the ICL limit our ability to detect them (see Ulmer et al. 1996; Adami et al. 2006, 2009).

It is not clear how UDGs were formed. It seems unlikely that they are the product of galaxy harassment (Moore et al. 1996) or tidal stirring (Mayer et al. 2001) of infalling galaxies: these processes tend to shrink galaxies, as the stars at larger radii are less bound than the stars at small radii (see, e.g., Mayer et al. 2001). A likely end-product of cluster-induced tidal effects are the ultra-compact dwarfs (Drinkwater et al. 2003), which have similar total luminosities and stellar masses as UDGs but stellar densities that are a factor of  $\sim 10^7$  higher.<sup>5</sup> We note, however, that the morphological evolution of infalling galaxies is difficult to predict, as it probably depends sensitively on the shape of the inner dark matter profile (e.g., Peñarrubia et al. 2010). An intriguing formation scenario is that UDGs are "failed"  $\sim L_*$  galaxies, which lost their gas after forming their first generation(s) of stars at high redshift (by ram pressure stripping or other effects). If this is the case they may have very high dark matter fractions, which could also help explain their survival in the cluster. Future studies of these objects, as well as counterparts in other clusters and in the field (see Dalcanton et al. 1997), may shed more light on these issues.

We thank the anonymous referee for an excellent and constructive report. We also thank the staff at New Mexico Skies for their support and Nelson Caldwell for comments on the manuscript. Support from NSF grant AST-1312376 is gratefully acknowledged.

#### REFERENCES

Abraham, R. G., & van Dokkum, P. G. 2014, PASP, 126, 55 Adami, C., Pelló, R., Ulmer, M. P., et al. 2009, A&A, 495, 407 Adami, C., Scheidegger, R., Ulmer, M., et al. 2006, A&A, 459, 679 Bertin, E., & Arnouts, S. 1996, A&AS, 117, 393 Bothun, G., Impey, C., & McGaugh, S. 1997, PASP, 109, 745 Bothun, G. D., Impey, C. D., & Malin, D. F. 1991, ApJ, 376, 404 Bovy, J., & Rix, H.-W. 2013, ApJ, 779, 115 Caldwell, N. 2006, ApJ, 651, 822 Chiboucas, K., Jacobs, B. A., Tully, R. B., & Karachentsev, I. D. 2013, AJ, 146, 126 Conroy, C., Gunn, J. E., & White, M. 2009, ApJ, 699, 486 Dalcanton, J. J., Spergel, D. N., Gunn, J. E., Schmidt, M., & Schneider, D. P. 1997, AJ, 114, 635 Doi, M., Fukugita, M., Okamura, S., & Turner, E. L. 1995, AJ, 109, 1490 Drinkwater, M. J., Gregg, M. D., Hilker, M., et al. 2003, Natur, 423, 519 Gavazzi, G., Donati, A., Cucciati, O., et al. 2005, A&A, 430, 411 Gavazzi, G., Fumagalli, M., Cucciati, O., & Boselli, A. 2010, A&A, 517, A73 Geha, M., Guhathakurta, P., & van der Marel, R. P. 2003, AJ, 126, 1794 Geller, M. J., Diaferio, A., & Kurtz, M. J. 1999, ApJL, 517, L23 Gregg, M. D., & West, M. J. 1998, Natur, 396, 549 Head, J. T. C. G., Lucey, J. R., Hudson, M. J., & Smith, R. J. 2014, MNRAS, 440, 1690 Heymans, C., Van Waerbeke, L., Miller, L., et al. 2012, MNRAS, 427, 146 Impey, C., Bothun, G., & Malin, D. 1988, ApJ, 330, 634 Kim, E., Kim, M., Hwang, N., et al. 2011, MNRAS, 412, 1881 Lelli, F., Fraternali, F., & Sancisi, R. 2010, A&A, 516, A11 Lieder, S., Lisker, T., Hilker, M., Misgeld, I., & Durrell, P. 2012, A&A, 538, A69 Macri, L. M., Hoffmann, S. L., Cook, K. H., et al. 2013, BAAS, 221, 152.06 Martel, H., Barai, P., & Brito, W. 2012, ApJ, 757, 48 Mayer, L., Governato, F., Colpi, M., et al. 2001, ApJ, 559, 754 McConnachie, A. W. 2012, AJ, 144, 4 McConnachie, A. W., Huxor, A., Martin, N. F., et al. 2008, ApJ, 688, 1009 Merritt, A., van Dokkum, P., & Abraham, R. 2014, ApJL, 787, L37 Michielsen, D., Boselli, A., Conselice, C. J., et al. 2008, MNRAS, 385, 1374

Mihos, J. C., Harding, P., Feldmeier, J., & Morrison, H. 2005, ApJL, 631, L41 Moore, B., Katz, N., Lake, G., Dressler, A., & Oemler, A. 1996, Natur,

Newman, A. B., Treu, T., Ellis, R. S., et al. 2013, ApJ, 765, 24

379, 613

<sup>5</sup> It is remarkable that both classes of objects exist in clusters at the same time.

Peñarrubia, J., Benson, A. J., Walker, M. G., et al. 2010, MNRAS, 406, 1290

Peng, C. Y., Ho, L. C., Impey, C. D., & Rix, H.-W. 2002, AJ, 124, 266
Schombert, J., McGaugh, S., & Maciel, T. 2013, AJ, 146, 41
Scoville, N., Aussel, H., Brusa, M., et al. 2007, ApJS, 172, 1
Shen, S., Mo, H. J., White, S. D. M., et al. 2003, MNRAS, 343, 978
Simard, L., Mendel, J. T., Patton, D. R., Ellison, S. L., & McConnachie, A. W. 2011, ApJS, 196, 11

Taylor, E. N., Hopkins, A. M., Baldry, I. K., et al. 2011, MNRAS, 418, 1587 Thompson, L. A., & Gregory, S. A. 1993, AJ, 106, 2197 Toloba, E., Guhathakurta, P., Boselli, A., et al. 2014, ApJ, submitted (arXiv:1410.1552)

Ulmer, M. P., Bernstein, G. M., Martin, D. R., et al. 1996, AJ, 112, 2517 van den Hoek, L. B., de Blok, W. J. G., van der Hulst, J. M., & de Jong, T. 2000, A&A, 357, 397

Vanderbeke, J., West, M. J., De Propris, R., et al. 2014, MNRAS, 437, 1734 van der Hulst, J. M., Skillman, E. D., Smith, T. R., et al. 1993, AJ, 106, 548 van Dokkum, P., & Conroy, C. 2014, ApJ, 797, 56 van Dokkum, P. G. 2001, PASP, 113, 1420

van Dokkum, P. G., Abraham, R., & Merritt, A. 2014, ApJL, 782, L24